01 Nov 1970

Phase Equilibria And Thermodynamic Studies In The System CaO-FeO-Fe2O3-SiO2

M. Timucin

Arthur E. Morris
Missouri University of Science and Technology

Recommended Citation

M. Timucin and A. E. Morris, "Phase Equilibria And Thermodynamic Studies In The System CaO-FeO-Fe2O3-SiO2," *Metallurgical Transactions*, vol. 1, no. 11, pp. 3193 - 3201, Springer, Nov 1970.
The definitive version is available at https://doi.org/10.1007/BF03038437

Phase Equilibria and Thermodynamic Studies in the System $CaO-FeO-Fe_2O_3-SiO_2$

M. TIMUCIN AND A. E. MORRIS

Phase equilibria and thermodynamic properties of the system $CaO-FeO-Fe_2O_3-SiO_2$ were studied at 1450° and 1550°C, over a range of pO_2 from 1 to about 10^{-11} atm. Isothermal phase diagrams and activity-composition diagrams were constructed for 0, 5, 10, 20, and 30 wt pct SiO_2 sections. The data are applicable to further understanding the behavior of simple BOF steelmaking slags.

IN order to provide a more complete basis for understanding the behavior of the slag formed in the basic oxygen furnace steel-making process, phase equilibria and activity measurements have been carried out over a wide range of compositions in the system $CaO-FeO-Fe_2O_3-SiO_2$, at 1450° and 1550°C. In particular, the work had the following objectives: 1) To determine the region of stability of certain solid phases in the $CaO-FeO-Fe_2O_3$ (ternary), and the $CaO-FeO-Fe_2O_3-SiO_2$ (quaternary) systems, 2) To determine the composition of liquid slags in the ternary and quaternary system, and 3) To calculate the activity-composition relationships of FeO, CaO, and SiO_2 in these systems.

Experimental work was carried out over a range of oxygen pressures from about 10^{-11} to 1 atm, at 1450° and 1550°C. Compositions in the ternary system were studied first, and then extended into the quaternary at 5, 10, 20, and 30 wt pct SiO_2 sections. Phase diagrams and activity diagrams for all sections studied were then constructed. The experimental data obtained in the present work was used as the basis for constructing the phase diagrams, except for certain compositions at 1550°C, mentioned later under Results.

EXPERIMENTAL METHOD

Phases in equilibrium were inferred from examination of samples quenched from the equilibration temperature. The samples were examined by metallographic and X-ray diffraction methods. The composition of all single-phase, and some two-phase samples was determined by chemical analysis.

The samples to be equilibrated were prepared from mixtures of various calcium silicates, calcium ferrites, iron silicates, lime, and silica. These starting materials had been previously prepared by reacting together reagent grade samples of $CaCO_3$, Fe_2O_3, and silicic acid, in appropriate amounts. Suitable precautions were taken to insure against segregation of sample, or loss of nonhomogeneous material, in all steps of sample preparation.

Samples of known composition were prepared for equilibration by packing about 0.8 g of the powdered sample into a thin-walled platinum or Pt-Rh crucible. The samples were heated for a minimum of 18 hr at 1450° and 8 hr at 1550°C; these times were found to be well in excess of that required for equilibration. Quenching was accomplished by dropping the samples into water or isopropyl alcohol (depending on the lime content), without disturbing the temperature or gas flow in the furnace.

The desired oxygen pressure (pO_2) was attained by passing various mixtures of O_2, N_2, CO, or CO_2, into the furnace, according to the procedure established by Darken and Gurry,[1] except that a Matheson gas proportioner was used to obtain the desired gas composition. Cylinders of premixed gases were often used, as supplied and analyzed by the Matheson Co. In general, gases were of sufficient purity to need no subsequent treatment, except for certain runs equilibrated at a pO_2 generated by the thermal decomposition of pure CO_2. In this case, Coleman Instrument grade CO_2 was further purified by passing over copper gauze at 550°C.

The pO_2 generated by CO/CO_2 mixtures at equilibrium temperature was calculated from thermodynamic data on the high temperature free energy of formation of CO_2 and CO[2]. The main uncertainty in calculation of the pO_2 was the error in reading the flowmeter tubes. For example, at 1450°C, the $\log(pO_2)$ was calculated to be -9.300 ± 0.005.

The vertical tube furnaces for sample equilibration were of conventional design, and controlled to ±2°C. The sample temperature was measured by a Pt-Pt/10 pct Rh thermocouple, which was standardized against the melting points of gold and palladium. The temperature of the sample was estimated to be correct to ±5°C.

The chemical composition of quenched samples was determined by analysis for divalent iron, total iron, and CaO, by well-known dichromate and permanganate potentiometric titrations. Silica was determined by difference. The accuracy of the analysis (and gas equilibration technique) was established by submitting samples to outside laboratories, and by analysis of $FeO-Fe_2O_3$ mixtures equilibrated under the conditions specified by Darken and Gurry.[3]

LITERATURE

A large amount of work has been reported on binary, ternary, and quaternary systems of relevance to the

M. TIMUCIN, formerly Graduate Student, Department of Metallurgical and Nuclear Engineering, University of Missouri-Rolla, Rolla, Mo., is Research Associate, Department of Geochemistry and Mineralogy, Pennsylvania State University, University Park, Pa. A. E. MORRIS is Associate Professor, Department of Metallurgical and Nuclear Engineering, University of Missouri-Rolla. The paper is based on a thesis submitted by M. TIMUCIN in partial fulfillment of the requirements of a Ph.D. degree from the University of Missouri-Rolla.

Manuscript submitted February 9, 1970.

present work. Of particular importance is the work by Muan and Osborn,[4] which contains most of the important phase diagrams, and discusses the theory and application of phase diagrams in steelmaking.

For the binary system Fe-O, the work of Darken and Gurry[1,3] has already been mentioned. Phase equilibria in the $CaO-SiO_2$ system has been summarized,[5] as has thermodynamic data on liquids and compounds.[6,7]

Phase equilibria in the system $CaO-FeO-Fe_2O_3$ has been surveyed by Muan and Osborn,[4] and an activity-composition diagram is available at 1550°C.[7] Turkdogan[8] has also calculated the activities of oxides in the above ternary, with results different than obtained in Ref. 7. Similar compilations of data in the system $FeO-Fe_2O_3-SiO_2$ are also available.[4,7,9-11]

Experimental data on the quaternary ($CaO-FeO-Fe_2O_3-SiO_2$) system is inadequate to construct a tetrahedral model. Phase diagrams have been constructed from experimental work, based on conditions in equilibrium with metallic iron and air.[4,12] The activity of "FeO" in a few slags, of compositions similar to those studied in the present work, has been presented.[7,13,14]

RESULTS

The experimental data are summarized in the form of isothermal phase diagrams for the ternary system, in Figs. 1 and 2 at 1450° and 1550°C, respectively. The compositions of the condensed phases are shown as a function of pO_2, and labeled on the diagram as "oxygen isobars." At 1450°, the Fe + liquid oxide phase boundary was determined from equilibrium runs in iron crucibles. At 1550°C, a lack of suitable crucible material for work along this boundary required the adoption of the data of Larson and Chipman.[14] The diagrams show, as expected, that the stability of magnetite decreases with increasing temperature. Hematite is completely unstable at all conditions studied in this work.

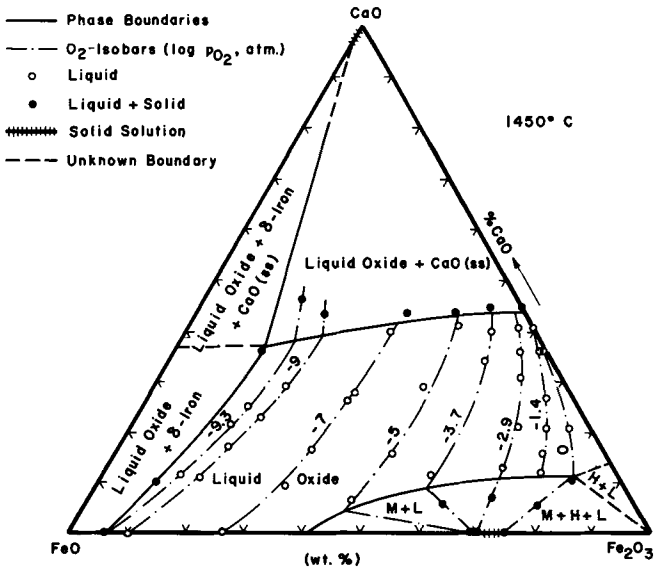

Fig. 1—The isothermal phase diagram for the $CaO-FeO-Fe_2O_3$ system. Abbreviations: M = magnetite, H = hematite, L = liquid oxide.

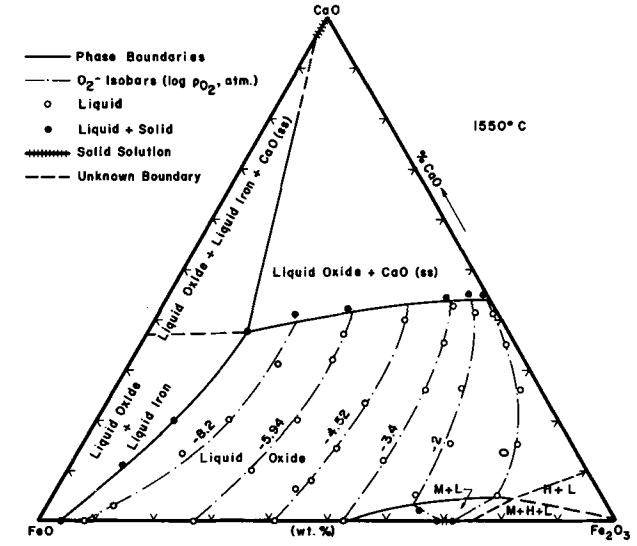

Fig. 2—The isothermal phase diagram for the $CaO-FeO-Fe_2O_3$ system. Abbreviations: M = magnetite, H = hematite, L = liquid.

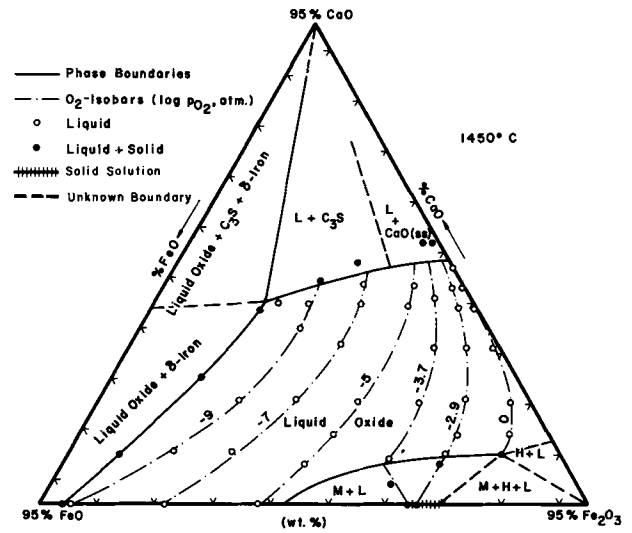

Fig. 3—The 5 pct SiO_2-isothermal phase diagram for the $CaO-FeO-Fe_2O_3-SiO_2$ system. Abbreviations: M = magnetite, H = hematite, L = liquid oxide, $C_3S = 3CaO \cdot SiO_2$.

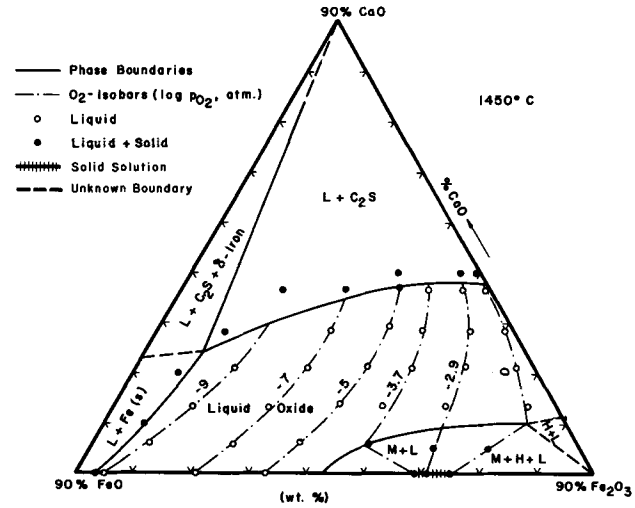

Fig. 4—The 10 pct SiO_2-isothermal phase diagram for the $CaO-FeO-Fe_2O_3-SiO_2$ system. Abbreviations: M = magnetite, H = hematite, L = liquid oxide, $C_2S = 2CaO \cdot SiO$.

The isothermal phase diagrams shown in Figs. 3 to 6 and 7 to 10 summarize the data at 1450° and 1550°C, respectively, at the 5, 10, 20, and 30 pct SiO_2 sections of the quaternary system. It should be pointed out that Figs. 3 to 10 are not true ternary systems. The use of "constant" pct SiO_2 sections to present the data means that the compositions of the crystalline phases in equilibrium with the liquid cannot be represented on the diagrams. The single-phase (liquid oxide melt) field and its immediate boundary curves are in the constant SiO_2 plane, however.

The 1550°C liquid Fe + liquid oxide phase boundaries were taken from Turkdogan,[9] and from interpolations between 1450°C of this work, and the 1600°C data of Taylor and Chipman.[15] The diagrams show that the stability of magnetite decreases with increasing silica. The stable crystalline phase in equilibrium with lime-saturated liquids is either CaO, containing a small amount of "FeO" in solid solution, tricalcium silicate, or dicalcium silicate. It is presumed that tricalcium silicate has a region of stability somewhere between 5 and 10 pct SiO_2 at 1550°C.

The shape of the oxygen isobars of Figs. 1 and 2 support the view that increasing the CaO content of an otherwise pure iron oxide melt tends to stabilize the trivalent iron,[4] and that this tendency decreases with

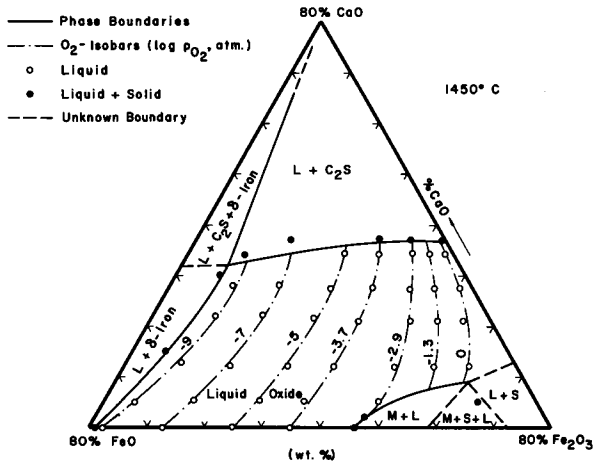

Fig. 5—The 20 pct SiO_2-isothermal phase diagram for the CaO-FeO-Fe_2O_3-SiO_2 system. Abbreviations: M = magnetite, S = silica, L = liquid oxide, C_2S = 2CaO · SiO_2.

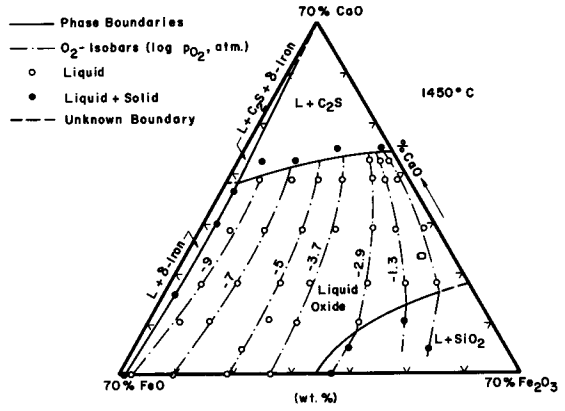

Fig. 6—The 30 pct SiO_2-isothermal phase diagram for the CaO-FeO-Fe_2O_3-SiO_2 system. Abbreviations: L = liquid oxide, C_2S = 2CaO · SiO_2.

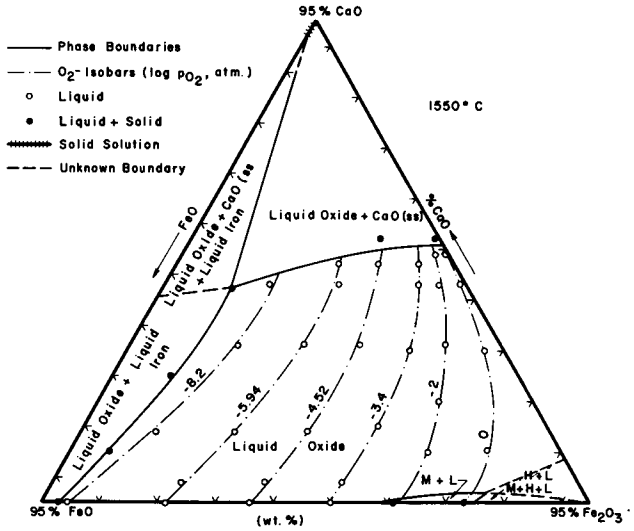

Fig. 7—The 5 pct SiO_2-isothermal phase diagram for the CaO-FeO-Fe_2O_3-SiO_2 system. Abbreviations: M = magnetite, H = hematite, L = liquid oxide.

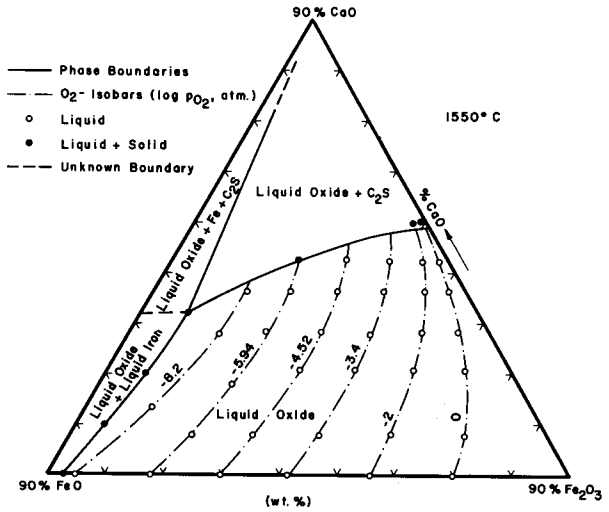

Fig. 8—The 10 pct SiO_2-isothermal phase diagram for the CaO-FeO-Fe_2O_3-SiO_2 system. Abbreviations: C_2S = 2CaO · SiO_2.

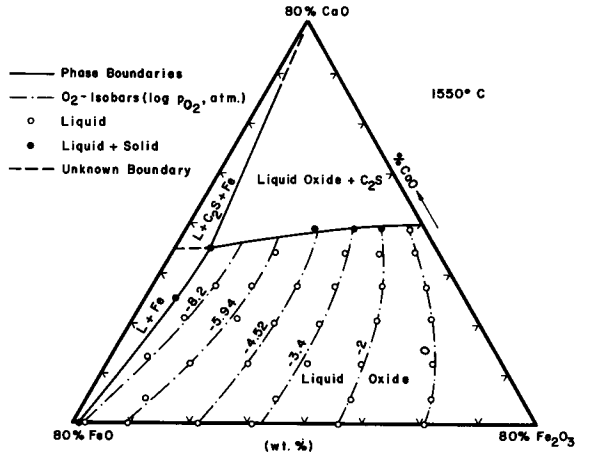

Fig. 9—The 20 pct SiO_2-isothermal phase diagram for the CaO-FeO-Fe_2O_3-SiO_2 system. Abbreviations: L = liquid oxide, C_2S = 2CaO · SiO_2.

increasing temperature. The data may be expressed as an arbitrarily defined stability parameter, and plotted as in Fig. 11, at two levels of CaO content, vs the log (pO_2). The addition of SiO_2 has the opposite effect of CaO, as shown by Fig. 12, where the same stability parameter is plotted for a melt containing 20 pct CaO at 1450°C. Obviously, the data can be used to plot a variety of other diagrams.

ACTIVITY CALCULATIONS

Ternary System

When the activity of one component of a ternary system is known, the activity of the other two can be calculated by ternary Gibbs-Duhem equations. Following the method described by Schuhmann,[16] the logarithm of the activity of component 2 at point II is given by:

$$\log a_2^{II} = \left\{ \log a_2^{I} - \int_{\log a_1^{I}}^{\log a_1^{II}} \left[\frac{\partial n_1}{\partial n_2}\right]_{a_1, n_3} d \log a_1 \right\}_{n_2/n_3} \quad [1]$$

where the activity of component 1 is known along the path of integration I-II (path of constant n_2/n_3). Fig. 13 illustrates the graphical determination of $[\partial n_1/\partial n_2]_{a_1,n_3}$ for a given point P in the I-II path, where the tangent intercept T may be either positive or negative. In a similar manner:

$$\log a_3^{II} = \left\{ \log a_3^{I} - \int_{\log a_1^{I}}^{\log a_1^{II}} \left[\frac{\partial n_1}{\partial n_3}\right]_{a_1, n_2} d \log a_1 \right\}_{n_2/n_3} \quad [2]$$

Along an isoactivity line of component 1, the Gibbs-Duhem equation reduces to an even simpler form. For example, if component 1 is oxygen, component 2 is iron, and component 3 is CaO, then along a line of constant oxygen activity (constant pO_2):

$$\log a_{CaO} = \left\{ \log a^{*}_{CaO} - \int_{\log a^{*}_{Fe}}^{\log a_{Fe}} \left(\frac{n_{Fe}}{n_{CaO}}\right) d \log a_{Fe} \right\}_{a_O} \quad [3]$$

where $\log a^{*}_{CaO}$ and $\log a^{*}_{Fe}$ values are equivalent to $\log a^{II}_{CaO}$ and $\log a^{II}_{Fe}$ values obtained by integrations of Eqs. [1] and [2] along path O-A, see Fig. 14.

The application of these equations to the CaO-FeO-Fe_2O_3 system have been described in detail by Turkdogan.[8] The method requires conversion of the data, as plotted in Figs. 1 and 2, to a CaO-Fe-O basis, as shown in Fig. 14. Thus, iron activities could be calculated along a number of paths of constant n_{Fe}/n_{CaO}, radiating from the O apex and terminating at the iron

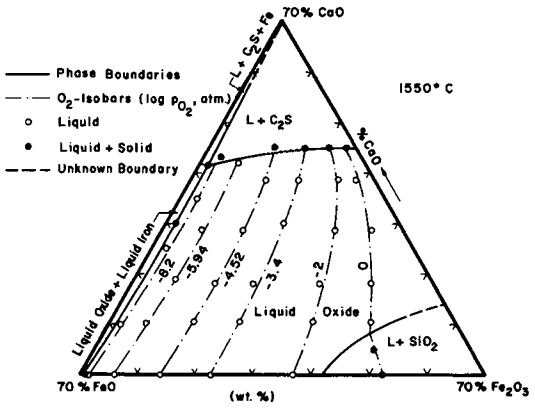

Fig. 10—The 30 pct SiO_2-isothermal phase diagram for the CaO-FeO-Fe_2O_3-SiO_2 system. Abbreviations: L = liquid oxide, C_2S = $2CaO \cdot SiO_2$.

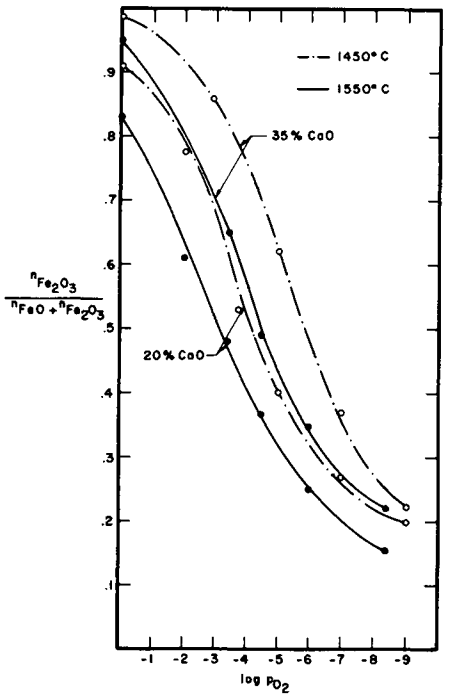

Fig. 11—The effect of temperature on the relative Fe^{3+} stability of the ternary CaO-FeO-Fe_2O_3 melts at two levels of CaO.

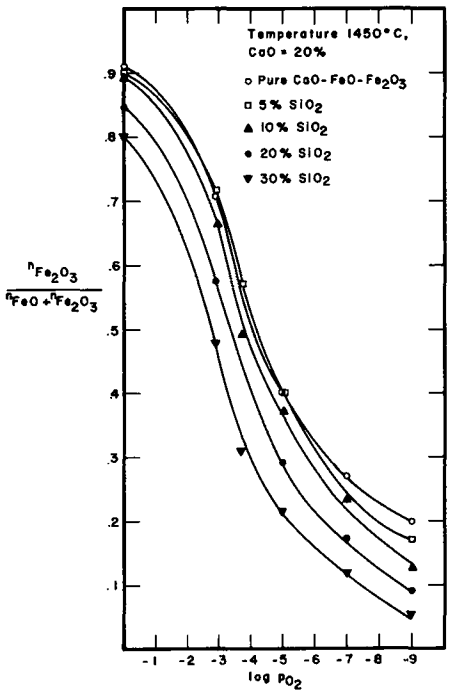

Fig. 12—The effect of silica additions on the relative Fe^{3+} stability of the CaO-FeO-Fe_2O_3-SiO_2 melts containing 20 pct CaO.

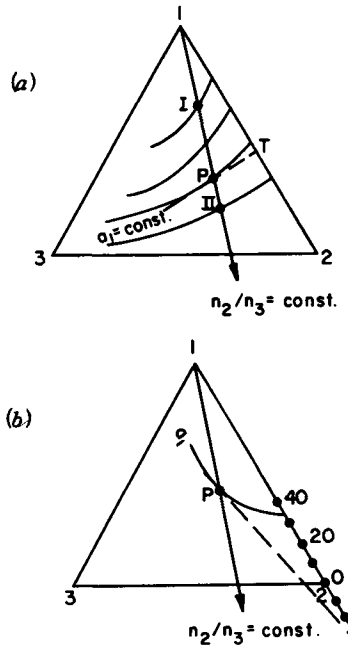

Fig. 13—Idealized composition triangle showing the construction of (*a*) positive tangent-intercepts, and (*b*) negative tangent-intercepts (T).

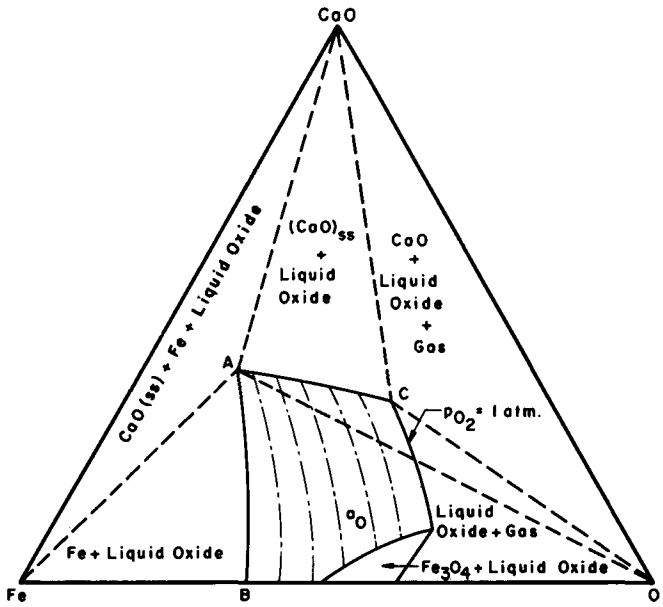

Fig. 14—Schematic CaO-Fe-O composition triangle showing the isooxygen activity curves.

saturation boundary where $\log a^{I}_{Fe} = 0$. The standard state for oxygen was defined as $pO_2 = 1$ atm, and the oxygen activity of the melt was defined as the $(pO_2)^{1/2}$ of the gas phase.

The "FeO" activity of the melt was evaluated by:

$$a_{\text{"FeO"}} = K(a_{Fe})(a_0) \qquad [4]$$

where the standard state for "FeO" was defined as the pure liquid iron oxide in equilibrium with metallic iron, at both temperatures. The value of K in Eq. [4] was 4.50×10^4 at 1450°C, and 1.87×10^4 at 1550°C.[3]

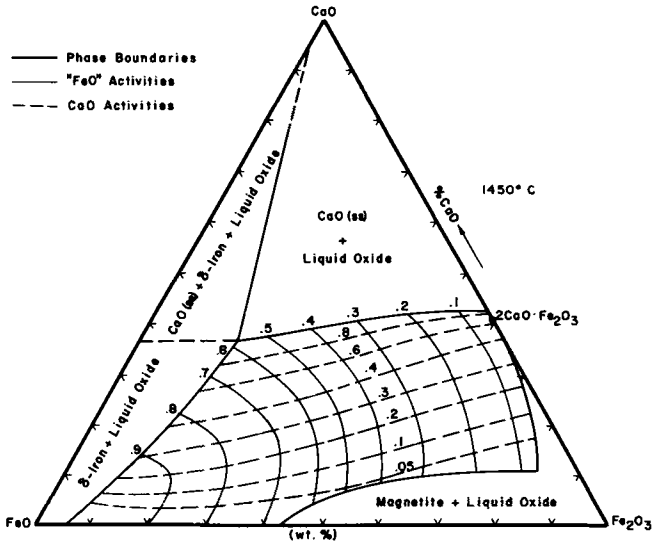

Fig. 15—Activities of "FeO" and CaO in melts of the system $CaO-FeO-Fe_2O_3$ at 1450°C.

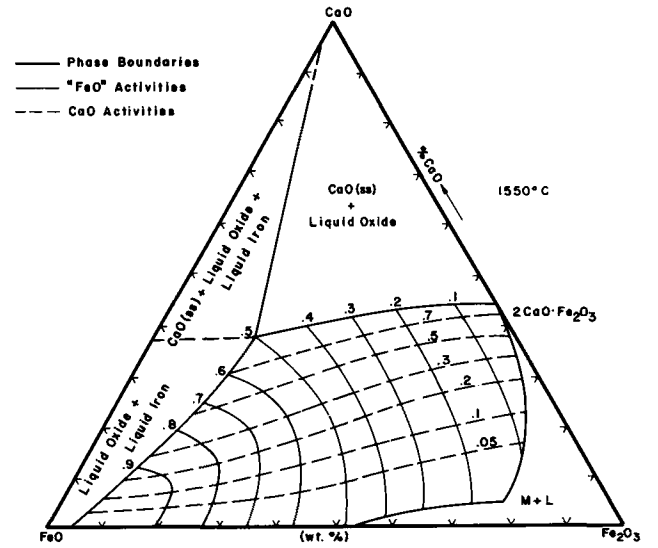

Fig. 16—Activities of "FeO" and CaO in melts of the system $CaO-FeO-Fe_2O_3$ at 1550°C.

Eq. [2] was used only once to determine the CaO activities along the path O-A, Fig. 14; at point A the $\log a^{I}_{CaO} = 0$, neglecting the effect of a small amount of "FeO" in solid solution. The rest of the CaO activities were calculated by Eq. [3], where $\log a^{*}_{CaO}$ values were those obtained from the previous integration of Eq. [2]. The activity of Fe_2O_3 was not calculated.

The activity of "FeO" and CaO are given in Figs. 15 and 16, as calculated from Eqs. [1] to [4]. The accuracy of the Fe activities at 1450°C were checked in two regions of the diagram: for liquids saturated with magnetite, and for the liquid in equilibrium with dicalcium ferrite.* For magnetite saturation (at 1450°C), the present work gave an average value of −136.2 kcal per mol for the standard free energy change of the follow-

*Dicalcium ferrite was found to melt at 1457°C at $pO_2 = 1$ atm. Since, within the limits of experimental error, the stability of $2CaO \cdot Fe_2O_3$ is very small or nonexistent, it was not shown on the isothermal phase diagram of Fig. 1.

ing reaction:

$$3Fe_{(s)} + 2O_2 \rightarrow Fe_3O_{4(s)} \quad [5]$$

The literature value[7] for the above reaction was -137.4 ± 2 kcal per mol.

For liquids saturated with dicalcium ferrite at 1450°C, the following two reactions were considered:

$$2CaO_{(s)} + Fe_2O_{3(s)} \rightarrow 2CaO \cdot Fe_2O_3 \quad [6]$$

$$2\text{"FeO"}_{(l)} + \tfrac{1}{2}O_{2(g)} \rightarrow Fe_2O_3 \quad [7]$$

If the value[7] of 2.32 for $\log K_{eq}$ for Eq. [7] is combined with values of $a_{\text{"FeO"}}$ and a_{CaO} from the present work (0.012 and 0.65, respectively) at the dicalcium ferrite point, a value of -15.9 kcal per mol is obtained for the standard free energy change accompanying Reaction [6]. This may be compared to a value of -16.7 ± 1 kcal per mol reported previously by other investigators.[17]

The "FeO" activity-composition relations obtained at 1550°C are in good agreement with the "FeO" activities of both Larson and Chipman[14] and Turkdogan.[8] The CaO activities at high-lime contents agree more closely to the values of Turkdogan, but their shapes resemble Chipman's curves. At low-lime contents, the CaO activities of Turkdogan are considerably lower than in the present work and that of Chipman. Both the magnetite and $CaO_{(ss)}$ boundaries are very similar to those of Turkdogan.

Quaternary System

Schuhmann's method for ternary Gibbs-Duhem integrations can be modified for systems of four or more components, as shown by Gokcen.[18] The following equations can be derived for the activities of iron, CaO, and SiO_2:

$$\log a^{II}_{Fe} = \left\{ \log a^{I}_{Fe} - \int_{\log a^{I}_{O}}^{\log a^{II}_{O}} \left[\frac{\partial n_O}{\partial n_{Fe}}\right]_{a_O,\ \frac{n_{CaO}}{n_{SiO_2}}} d \log a_O \right\}_{\frac{n_{CaO}}{n_{SiO_2}},\ \frac{n_{Fe}}{n_{CaO}}} \quad [8]$$

$$\log a^{II}_{SiO_2} = \left\{ \log a^{I}_{SiO_2} - \int_{\log a^{I}_{O}}^{\log a^{II}_{O}} \left[\frac{\partial n_O}{\partial n_{SiO_2}}\right]_{a_O,\ \frac{n_{Fe}}{n_{CaO}}} d \log a_O \right\}_{\frac{n_{Fe}}{n_{SiO_2}},\ \frac{n_{Fe}}{n_{CaO}}} \quad [9]$$

$$\log a^{II}_{CaO} = \left[\log a^{I}_{CaO} - \int_{\log a^{I}_{Fe}}^{\log a^{II}_{Fe}} \frac{n_{Fe}}{n_{CaO}} d \log a_{Fe} - \int_{\log a^{I}_{O}}^{\log a^{II}_{O}} \frac{n_O}{n_{CaO}} d \log a_O \right]_{a_{SiO_2}} \quad [10]$$

The calculation of iron activities by Eq. [8] calls for converting the compositions to a $CaO-SiO_2-Fe-O$ basis, and measuring the tangent intercept values n_O/n_{Fe} along several n_{Fe}/n_{CaO} compositional paths that lie in planes of constant n_{CaO}/n_{SiO_2} ratio. These paths originate from the O apex of the composition tetrahedron, and terminate at the iron saturation boundary where $\log a^{I}_{Fe} = 0$. The "FeO" activities could then be calculated by Eq. [4], by using the appropriate values of K.

The procedure of determining the SiO_2 activities is very similar to that of iron, except the tangent intercepts must be measured along n_{Fe}/n_{SiO_2} paths that lie in planes of constant n_{Fe}/n_{CaO} ratio. The CaO activities were obtained from a relatively simple Gibbs-Duhem integration, by using the known iron and oxygen activities, and Eq. [10].

Obviously, the complete evaluation of the activities of SiO_2 and CaO depends on having accurate values for their activities at the start of the integration path, $\log a^{I}_{i}$ in Eq. [1]. For the present situation, the quaternary $CaO-SiO_2-Fe-O$ system could be satisfactorily approximated to the ternary $CaO-\text{"FeO"}-SiO_2$ system (in contact with metallic iron) insofar as the $\log a^{I}_{i}$ values represented the situation when activities had to be known along the iron-saturation boundary. The "FeO" activities in Figs. 17 and 18 were plotted at 1450° and 1550°C, after expressing divalent and trivalent iron as total FeO, and converting all compositions to mol fractions. The SiO_2 activities in the composition field X-Y-FeO_t could be calculated from the graphical integration of:

$$\log a^{I}_{SiO_2} = \left\{ \log a^{*}_{SiO_2} - \int_{a^{*}_{\text{"FeO"}}}^{a^{I}_{\text{"FeO"}}} \left[\frac{\partial n_{FeO}}{\partial n_{SiO_2}}\right] d \log a_{\text{"FeO"}} \right\}_{n_{CaO}/n_{SiO_2}} \quad [11]$$

The standard state for SiO_2 was defined as pure, solid silica, hence $\log a^{*}_{SiO_2} = 0$ at the silica saturation boundary. The extension of isosilica activities to the CaO-

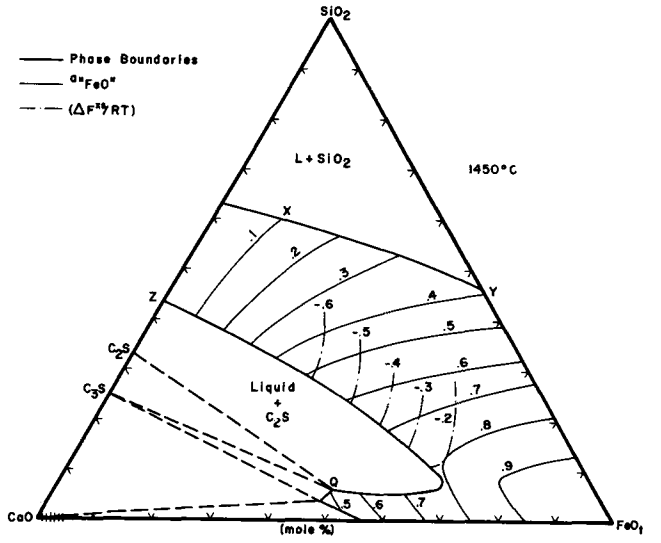

Fig. 17—"FeO" activities and the excess molar free energies of mixing in melts of the system $CaO-\text{"FeO"}-SiO_2$ at 1450°C.

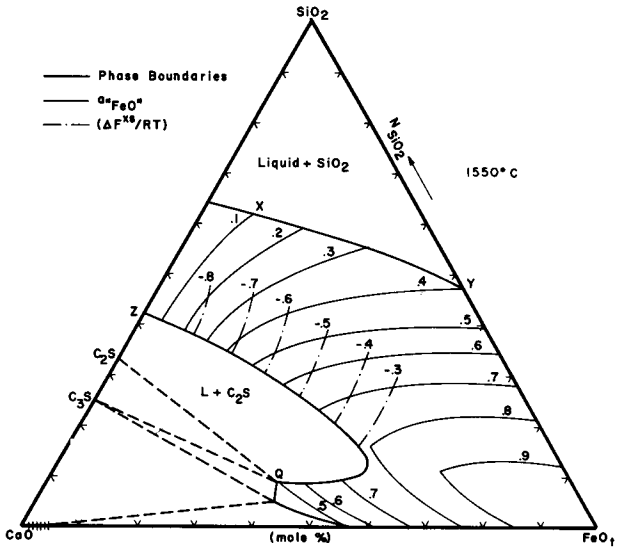

Fig. 18—"FeO" activities and the excess molar free energies of mixing in melts of the system CaO-"FeO"-SiO_2 at 1550°C.

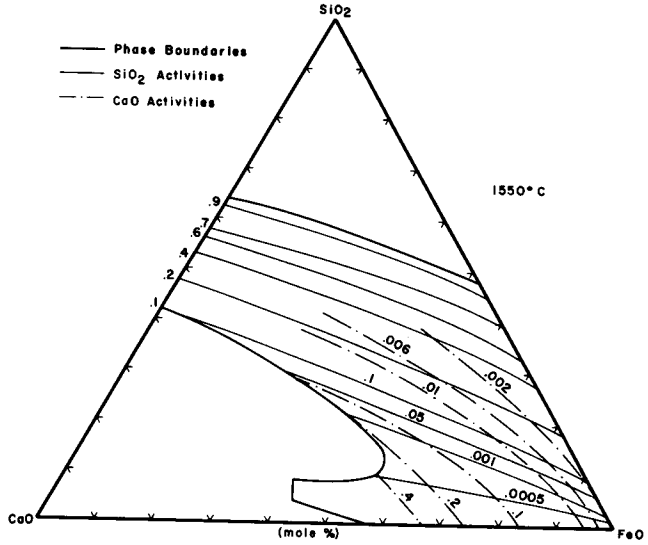

Fig. 20—CaO and SiO_2 activities in melts of the system CaO-"FeO"-SiO_2 at 1550°C.

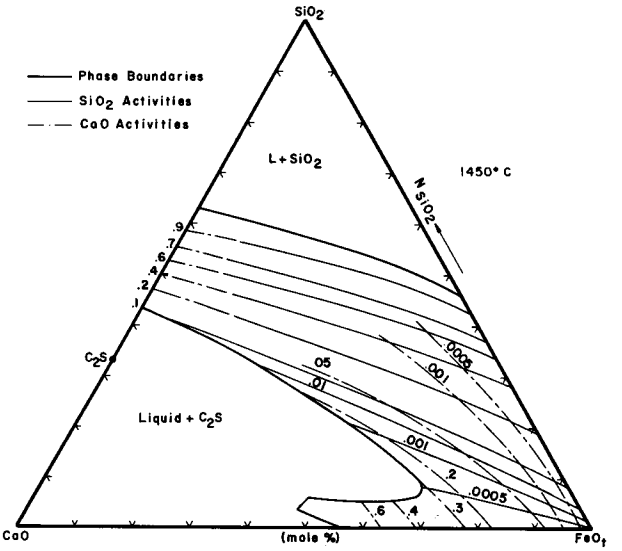

Fig. 19—CaO and SiO_2 activities in melts of the system CaO-"FeO"-SiO_2 at 1450°C.

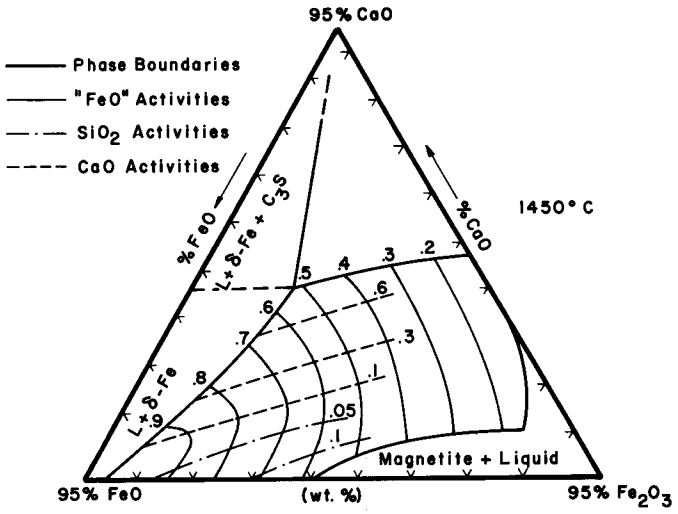

Fig. 21—Activities of "FeO", CaO, and SiO_2 in melts of the system CaO-FeO-Fe_2O_3-SiO_2 in the 5 pct SiO_2 section at 1450°C.

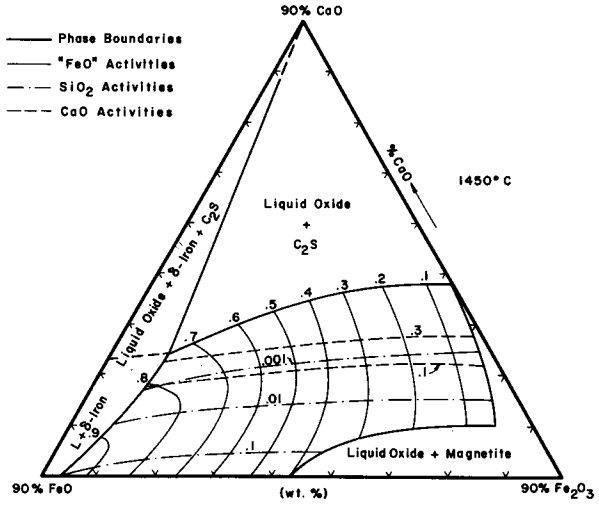

Fig. 22—Activities of "FeO", CaO, and SiO_2 in melts of the system CaO-FeO-Fe_2O_3-SiO_2 in the 10 pct SiO_2 section at 1450°C.

SiO_2 binary (in the range where $a^{I}_{SiO_2}$ = 1.0 to 0.4) resulted in SiO_2 activities which were in good agreement with those of Taylor and coworkers[19,20] along the CaO-SiO_2 join. Their results were therefore adopted for all compositions of interest along the join, at both temperatures.

For compositions below the line Z-FeO_t, Schuhmann's method was inapplicable. For SiO_2 activities below 0.1, calculations were made using Darken's equation:[21]

$$\Delta F^{xs}_t = RT(1-N_{FeO}) \times \left[\Delta F^{xs}_b + \int_0^{N_{FeO}} \frac{1n\gamma FeO}{(1-N_{FeO})^2} dN_{FeO}\right]_{N_{CaO}/N_{SiO_2}} \quad [12]$$

where: ΔF^{xs}_t is the ternary excess molar free energy

of mixing, and is given by:

$$\Delta F_t^{xs} = RT(N_{CaO} \cdot \log\gamma_{CaO} + N_{SiO_2} \cdot \log\gamma_{SiO_2} + N_{FeO} \cdot \log\gamma_{FeO}) \quad [13]$$

and ΔF_b^{xs} = excess molar free energy of mixing in the $CaO\text{-}SiO_2$ binary.

Values of F_t^{xs}/RT could be calculated along a number of paths of constant N_{CaO}/N_{SiO_2} near the dicalcium silicate saturation boundary, from plots like those shown in Figs. 15 and 16. The SiO_2 and CaO activities along this boundary were then obtained by simultaneous solution of Eq. [13] and Eq. [14].

$$2CaO_{(s)} + SiO_{2(s)} \rightarrow 2CaO \cdot SiO_2$$

$$\text{Log } K = -2 \log a_{CaO} - \log a_{SiO_2} \quad [14]$$

Values of $\log K$ for Eq. [14] were 4.08 and 4.25 at 1450° and 1550°C, respectively.[7]

The low-SiO_2 activities shown in Figs. 19 and 20 were drawn by joining values calculated at the dicalcium silicate boundary, with those values of a_{SiO_2} on the FeO-SiO_2 binary as inferred from the work of Turkdogan[9] and Schuhmann and Ensio.[22] The CaO activities in the ternary field were calculated by:

$$\log a_{CaO}^{I} = \left[\log a_{CaO}^{*} - \int_{a_{SiO_2}^{*}}^{a_{SiO_2}^{I}} \frac{n_{SiO_2}}{n_{CaO}} d\log a_{SiO_2}\right]_{a_{"FeO"}} \quad [15]$$

The a_{CaO}^{*} and $a_{SiO_2}^{*}$ values were those at the dicalcium silicate saturation boundary.

The activity-composition relations in the quaternary melts are shown in Figs. 21 through 28. The data used to construct these figures can be expressed in many other ways, depending on which variables are of greatest interest. Fig. 29, for example, shows the effect of increased SiO_2 content on "FeO" activities in a quaternary melt containing 15 pct CaO at 1450°C.

The accuracy of the activity calculations is affected by the extrapolations discussed earlier, to SiO_2 con-

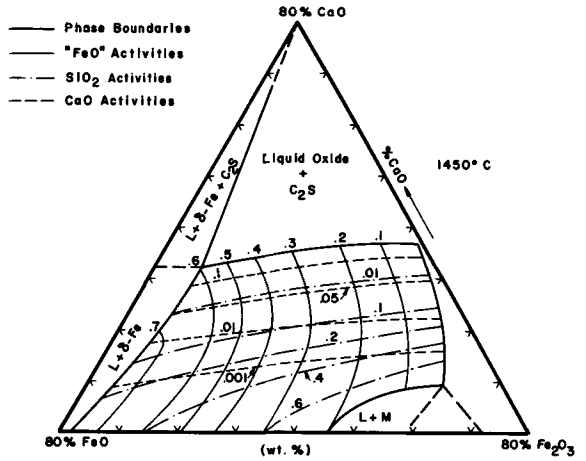

Fig. 23—Activities of "FeO", CaO, and SiO_2 in melts of the system $CaO\text{-}FeO\text{-}Fe_2O_3\text{-}SiO_2$ in the 20 pct SiO_2 section at 1450°C.

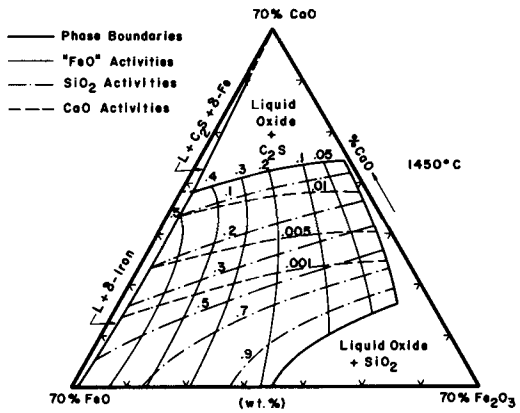

Fig. 24—Activities of "FeO", CaO, and SiO_2 in melts of the system $CaO\text{-}FeO\text{-}Fe_2O_3\text{-}SiO_2$ in the 30 pct SiO_2 section at 1450°C.

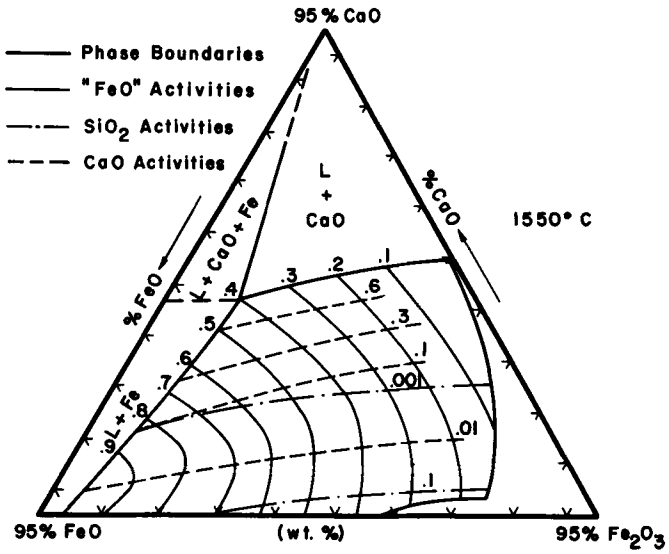

Fig. 25—Activities of "FeO", CaO, and SiO_2 in melts of the system $CaO\text{-}FeO\text{-}Fe_2O_3\text{-}SiO_2$ in the 5 pct SiO_2 section at 1550°C.

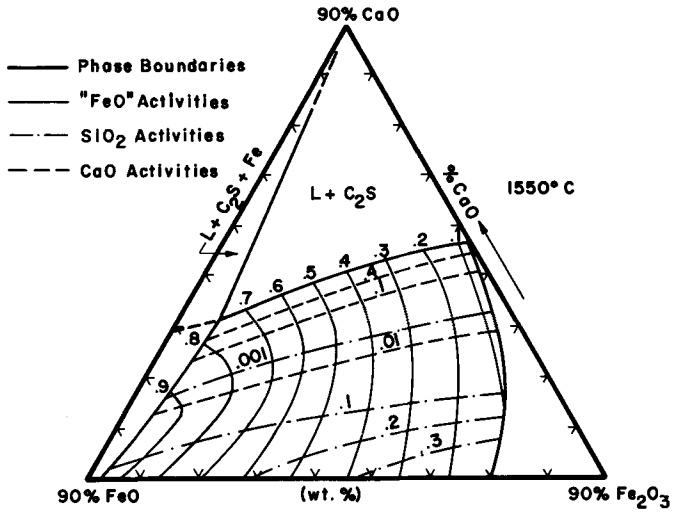

Fig. 26—Activities of "FeO", CaO, and SiO_2 in melts of the system $CaO\text{-}FeO\text{-}Fe_2O_3\text{-}SiO_2$ in the 10 pct SiO_2 section at 1550°C.

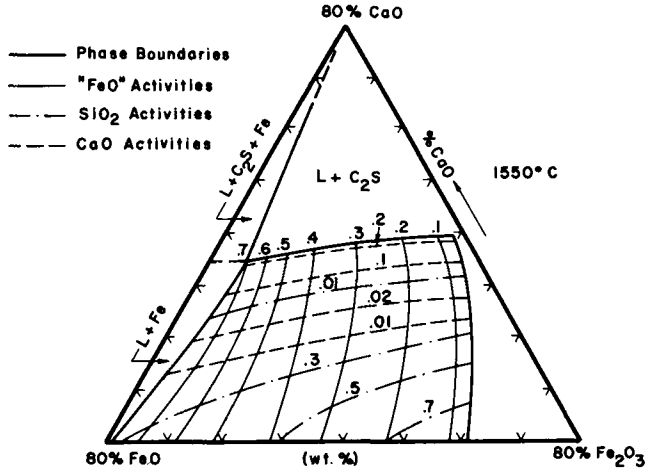

Fig. 27—Activities of "FeO", CaO, and SiO_2 in melts of the system CaO-FeO-Fe_2O_3-SiO_2 in the 20 pct SiO_2 section at 1550°C.

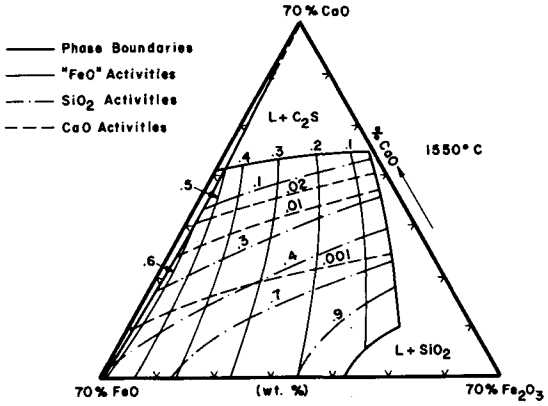

Fig. 28—Activities of "FeO", CaO, and SiO_2 in melts of the system CaO-FeO-Fe_2O_3-SiO_2 in the 30 pct SiO_2 section at 1550°C.

tents above 30 pct. Our values for the activity of "FeO" at 1550°C are in good agreement with those of Larson and Chipman[14] up to 10 pct SiO_2, and slightly lower than theirs at higher silica. As in the ternary melts, the activity of "FeO" could be checked against the value of ΔF° for Reaction [5] at 1450°C. The average values of ΔF° (kcal per mol) obtained were: −134.0, −136.6, and −138.6, at the 5, 10, and 20 pct SiO_2 sections, respectively. The accuracy in the calculation for the activity of "FeO" improves at higher SiO_2 contents because of the nature of Eq. [8].

SUMMARY

The phase equilibria and activity-composition relations have been determined in the CaO-FeO-Fe_2O_3 systems at 1450° and 1550°C, for SiO_2 contents in the range 0 to 30 wt pct. The diagrams* provide quantitative information on the affect of composition, temperature, and pO_2, on the ability of a simple BOF slag to act as a transfer medium for oxygen to the bath. The data obtained are in good agreement with existing data, and extend knowledge of the system into regions not previously studied.

*Enlarged ternary diagrams are available on request from one of the authors (A.E.M.).

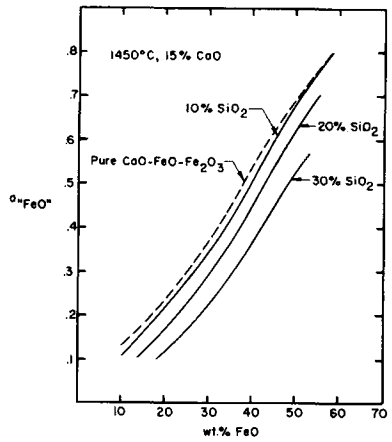

Fig. 29—Effect of increasing SiO_2 addition on "FeO" activities of CaO-FeO-Fe_2O_3-SiO_2 melts containing 15 pct CaO at 1450°C.

ACKNOWLEDGMENTS

We are grateful to the National Lime Association for their sponsorship of this work, and to UNESCO for a fellowship.

REFERENCES

1. L. S. Darken and R. W. Gurry: *J. Am. Chem. Soc.*, 1945, vol. 67, pp. 1398-1412.
2. Richard A. Robie and D. R. Waldbaum: *U. S. Geol. Surv. Bull. 1259*, 1968.
3. L. S. Darken and R. W. Gurry: *J. Am. Chem. Soc.*, 1946, vol. 68, pp. 798-816.
4. A. Muan and E. F. Osborn: *Phase Equilibria Among Oxides in Steelmaking*, Addison-Wesley Publishing Co., Reading, Mass., 1965.
5. Ernest M. Levin, C. R. Robbins, and H. F. McMurdie: *Phase Diagrams for Ceramists*, The American Ceramic Society, Columbus, Ohio, 1964.
6. K. K. Kelley: *U. S. Bur. Mines Rept. Invest., 5901*, 1962.
7. J. F. Elliott, M. Gleiser, and V. Ramakrishna: *Thermochemistry for Steelmaking, Volume II*, Addison-Wesley Publishing Co., Reading, Mass., 1963.
8. E. T. Turkdogan: *Trans. TMS-AIME*, 1961, vol. 221, pp. 1090-95.
9. E. T. Turkdogan: *Trans. TMS-AIME*, 1962, vol. 224, pp. 294-98.
10. J. White: *J. Iron Steel Inst., Carnegie Schol. Mem.*, 1938, vol. 27, pp. 1-75.
11. E. T. Turkdogan and P. M. Bills: *J. Iron Steel Inst.*, 1957, vol. 186, pp. 329-39.
12. *Phase Equilibria Diagrams of Oxide Systems:* Plates 7 and 10, The American Ceramic Society, Columbus, Ohio, 1960.
13. E. Görl, F. Oeters, and R. Scheel: *Arch. Eisenhuettenw.*, 1966, vol. 37, pp. 441-51.
14. H. Larson and J. Chipman: *AIME Trans.*, 1954, vol. 200, pp. 759-92.
15. C. R. Taylor and J. Chipman: *AIME Trans.*, 1943, vol. 154, pp. 228-47.
16. R. Schuhmann, Jr.: *Acta Met.*, 1955, vol. 3, pp. 219-26.
17. M. F. Koehler, B. Barany, and K. K. Kelley: *U. S. Bur. Mines Rept. Invest., 5711*, 1961.
18. N. A. Gokcen: *J. Phys. Chem.*, 1960, vol. 64, pp. 401-06.
19. J. D. Baird and J. Taylor: *Trans. Faraday Soc.*, 1958, vol. 54, pp. 526-39.
20. D. A. R. Kay and J. Taylor: *Trans. Faraday Soc.*, 1960, vol. 56, pp. 1372-86.
21. L. S. Darken: *J. Am. Chem. Soc.*, 1950, vol. 72, pp. 2909-14.
22. R. Schuhmann, Jr., and P. J. Ensio: *AIME Trans.*, 1951, vol. 191, pp. 401-11.